Contents list available at IJRED website

International Journal of Renewable Energy Development

Journal homepage: https://ijred.undip.ac.id

Research Article

Screen printed carbon electrode from coconut shell char for lead ions detection

Kinkind Raras Heliani[1,2], Fitria Rahmawati[1*], Agung Tri Wijayanta[3]

[1]*Research Group of Solid-State Chemistry and Catalysis, Chemistry Department, Sebelas Maret University, Indonesia*

[2]*Chemistry Department, Faculty of Mathematics and Natural Sciences, Sebelas Maret University, Indonesia*

[3]*Research Group of Sustainable Thermofluids, Mechanical Engineering, Sebelas Maret University, Indonesia*

Abstract. This research aimed to produce a screen-printed carbon electrode (SPCE) from an activated coconut shell carbon. As a raw material, coconut shell char provides renewability and is abundantly available in the market. Meanwhile, SPCE offers a simple electroanalytical electrode because the working, counter, and reference electrodes are in one piece. The coconut shell carbon was activated by steam at 700 °C for 1h, producing AC700 that was then characterized to ensure the result by following per under carbon as the main component, the phases, crystal structure, surface area, morphology, and elemental content. The result showed that the surface area of AC700 is 816 m^2/g, and the surface structure is porous, as identified by SEM images. Impedance analysis followed by data fitting and conductivity calculation found a high conductivity of 8.68 x 10^{-2} Scm^{-1}. The produced-SPCE or SPAC700 was modified by ferrocene at various compositions of 10%; 20%; and 30% of mass. The SPAC700-Fc30 provided the best performance for lead analysis with a detection limit of 0.35 mM, a quantitation limit of 1.17 mM, and good reproducibility with a Repeatability Coefficient (RC) of 0.022. SPAC700-Fc30 showed good lead ions detection despite under 10% Cu^{2+} and 10% Co^{2+} interferences. The result confirmed the potential use of coconut shell char as the raw material for SPCE production.

Keywords: Coconut Shell, Activated Carbon, SPCE, Ferrocene, lead - ions analysis

Received: 25th August 2023; Revised: 5th Nov 2023; Accepted: 10th Nov 2023; Available online: 20th Nov 2023

1. Introduction

Coconut shell is a solid waste that contains 93.51% Carbon,6.26%, Oxygen and some minerals such as K and Si at 0.18% and 0.13%, respectively (Nita *et al.*, 2021). The identified elements exist in some macro-molecules, including pentose at 27.7%, cellulose at 26.6%, lignin at 29.4%, water at 8%, hexuronic acid anhydrous at 3.5%, a 4.2% of other volatile organic compounds and 0.6% ash (Rizal *et al.*, 2020). The significant carbon content made the coconut shell a promising candidate for carbon production. Carbon powder, which physical or chemical methods can be activated, is essential for various applications, including water vapor adsorption (Ridassepri *et al.*, 2020), methylene blue adsorption (Rahmawati *et al.*, 2021), photoelectrodes (Imani *et al.*, 2022), photo-electrocatalytic (Su *et al.*, 2020), as anode for lithium-ion batteries (Mopoung *et al.*, 2021), as electrode material on capacitors (Kuan-Ching Lee *et al.*, 2021) and also screen printing carbon electrode (Ahammad *et al.*, 2019). The quality of produced activated carbon is the crucial thing for many applications.

Activation is a crucial step to increase carbon performance. Recently, physical activation is preferable for environmental safety reasons. Physical activation is usually conducted by flowing gas such as water vapor, CO_2, or N_2 while a high temperature is applied (Rahmawati *et al.*, 2021; Khuong *et al.*, 2021; Rezma *et al.*, 2017). Steam or water vapor is preferable by following the cost and its ability to increase the surface area of the activated carbon (Chairunnisa et al., 2021; Hidayat & Sutrisno, 2016) , which can reach up to 946.5m^2/g (Widanarto *et al.*, 2022). Surface area is an essential parameter for adsorption and reaction scene on the carbon surface, including for electrochemical reaction, while carbon is used as a working electrode.

Some carbon based-electrode for electrochemical cell and electroanalysis are glassy carbon electrodes (GCE) for Cd^{2+} and Pb^{2+} analysis (Mao *et al.*, 2022), GCE modified with Bi-film organic framework and polypyrrole (BF-PPy/MOF/GCE) for Pb^{2+} analysis (Y. Liu *et al.*, 2022), GCE modified with graphitic carbon nitride (g-C_3N_4) and tin dioxide nanoparticles (SnO_2/g-C_3N_4/GCE) for Cd^{2+} analysis (Z. Liu *et al.*, 2023), magnetic activated carbon (MAC) modified with cobalt nanocomposite (MAC-Co-SPCE) for Bisphenol A analysis (Emambakhsh *et al.*, 2022), and carbon paste electrode (CPE) modified with ferrocene (Fc/CPE) for dopamine analysis (Widyaningrum *et al.*, 2020).

However, research on carbon electrodes derived from biomass is still limited, such as CPE from walnut shell biochar for simultaneous detection of heavy metal ions in water (El Hamdouni *et al.*, 2022), and GCE from leaves of lettuce for black carbon, modified using $CuCo_2O_4$ was combined with

* Corresponding author
Email: fitria@mipa.uns.ac.id (F. Rahmawati)

https://doi.org/10.14710/ijred.2024.57679
ISSN: 2252-4940/© 2024.The Author(s). Published by CBIORE

molecularly imprinted polymer (MIP/ $CuCo_2O_4$-BC/GCE) for tryptophan analysis (Chen *et al*., 2021). Screen-Printed Carbon Electrode (SPCE) is another form of carbon electrode that unifies working, counter, and reference electrode in a piece. The SPCE modified with Ferrocene, Fc, shows good performance for drug analysis by electrochemical volumetric method (Ren et al., 2021). Our previous research used bagasse, a solid waste of a sugarcane factory, for SPCE production, shows good performance for Cu^{2+} electroanalysis (Rahmawati *et al*., 2023). However, factories usually process the sugarcane only twice a year, allowing less sustainability of bagasse once mass production of SPCE is planned.

Coconut shell char is a suitable replacement for bagasse due to its abundance, sustainability, and availability in the market because coconut is the main component for dishes and drinks in tropical countries. Therefore, this research used coconut shell char to prepare SPCE. The coconut shell carbon powder was also activated by steam (Rahmawati et al., 2023) instead of chemical activation, considering the environmental safety and friendly. The SPCE produced from the produced-activated carbon was modified with ferrocene to increase its performance as the electrode for Pb^{2+} by voltametric analysis. Analysis of Lead, Pb^{2+} is important because lead is a toxic metal that may present in municipal water systems due to corrosion of lead pipes or lead solder of pipe joints (H. Nguyen et al., 2018). Lead poisoning and environmental lead pollution can also be caused by the paint, automobile, and pottery industries (Jagirani et al., 2022). Being exposed to water and consuming lead-contaminated water, even at a trace levels may harm human health, especially for children(Q. Wang et al., 2009). This research aims to prepare SPCE from activated coconut shell carbon and examine its performance as a simple electrode for Pb^{2+} electroanalysis.

2. Material and method

2.1 Material preparation

This research used coconut shell char procured from a char producer (Klaten, Central Java, Indonesia). The char was crushed into powder and was filtered at 100 mesh size. The 100-mesh powder was washed and soaked in distilled water for 1 h under stirring conditions. After water decantation, the wet powder was dried at 60 °C for 1 h in an oven.

2.2 Char analysis

The result char was black-smooth powder, which then being analyzed by X-Ray diffraction (XRD) analyses at 0° – 80° (Rigaku Minifex 600 Cu/Ka) to understand its specific diffraction pattern, FTIR analysis (Shimadzu IR Prestige-2) at 4000-400 cm-1 wavenumber to analyze its functional groups vibration, Raman Spectroscopy (Raman iHR320 HORIBA) to determine the structural properties at the nanometric scale. Meanwhile, the surface area, pore volume, and pore distribution were analyzed by Surface Area Analyzer (SAA) (Quantachrome Instruments TouchWin V1.2 Tipe NOVA Touch 4LX), through adsorption–desorption of N2 gas at 77 K and relative pressure.

2.3 Char Activation and Characterization

For the activation process, the 100-mesh carbon powder was subjected to firing in a furnace at 700 °C for 1 h with a heating rate of 5 °C/min under steam flow. The activation was conducted within an installed-tube furnace as described in Fig. 1. A boiled water produced steam that flowed into the furnace

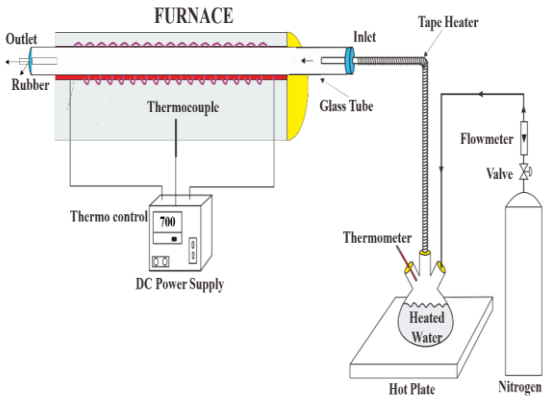

Fig.1 Scheme of the installed-tube furnace for steam activation

along with the N_2 gas carrier. The resulting-activated powder, AC700, was analytically weighted to calculate % yield by applying equation (1) followed by XRD, FTIR, SAA, Raman, and SEM/EDX (JSM-6510LA) analysis.

$$\%\ yield = \frac{weight\ of\ AC700}{weight\ of\ char} \times 100 \qquad (1)$$

.

2.4 Preparation of screen-printed carbon electrode (SPCE)

The mixture AC700, conductive agent (acetylene black), and polyvinylidene fluoride, PVDF binder under a mass ratio of 7:2:1 was dispersed in 4 mL of N-Methyl 2- Pyrrolidone, NMP (Huang et al., 2021), and was stirred continuously until homogeneous. The SPCE pattern (Figure 2 (a)) was printed on polyvinyl chloride (PVC) paper by Epson L210 series. The AC700 slurry was then applied to the SPCE pattern following the black area, as shown in Fig. 2(a). The SPCE was then heated in a vacuum oven at 50°C for 5 min to obtain good adhesion between the activated carbon ink and the PVC substrate (Rahmawati et al., 2023; Wahyuni et al., 2021). After drying, silver paste was painted on the reference part and half-length of working and counter electrode (Fig. 2 (b)) and then applied paraffin liquid on the surface of those three electrode parts to ensure that the three electrodes did not come short contact (Fig. 2c). The results were screen-printed carbon electrode from AC700 or SPAC700. The SPAC700 was then modified by adding ferrocene solution on the working electrode part at 10, 20, and 30 % mass to produce SPAC700-Fc10, SPAC700-Fc20, and SPAC700-Fc30, respectively. The electrochemical behavior of SPAC700 was investigated by conducting cyclic voltammetry (CorrTest electrochemical workstation CS50) with Pb (II) solution as analyte. Similar work was done for a commercial SPCE for control. All electrochemical measurement was conducted triple.

2.5 Electrochemical test

The SPAC700 or the SPAC700-Fc was attached to the electrode socket and dipped into $Pb(NO_3)_2$ solution as described by Fig.3. The preparation was done in an argon glove box (CY-VGB-1 with Ultra High Pure (UHP) Argon gas from PT. Samator Gas Indonesia) to prevent oxygen disturbance during measurement. To check the optimum ferrocene percentage, the SPAC700, which was modified by various 10%, 20%, and 30% Ferrocene, has applied to 0.2 mM $Pb(NO_3)_2$ solution and

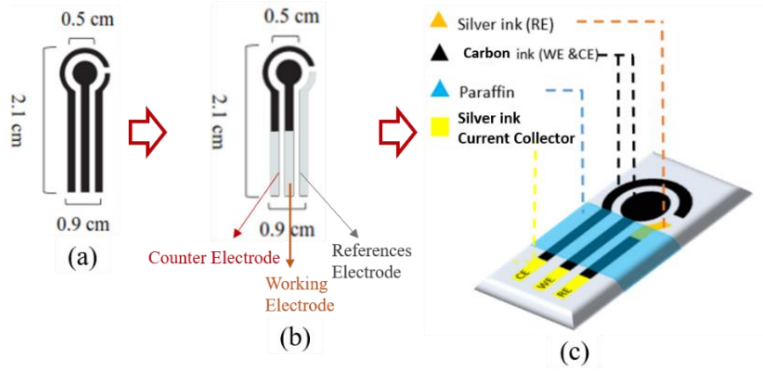

Fig.2 The Scheme of SPCE pattern (a), SPCE with the applied-Ag paste (b), SPCE with the applied-paraffin oil

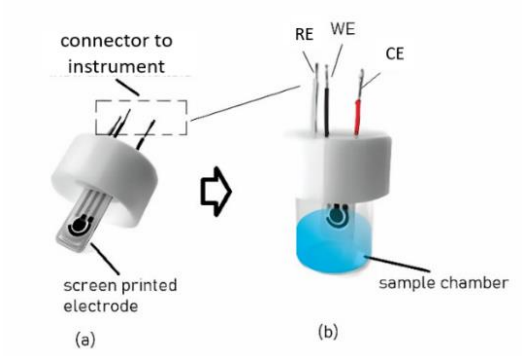

Fig 3. The SPCE socket **(a)** and the assembled-socket with the analyte solution chamber **(b)**

objected to CV analysis at −1.5 to 1 V vs Ag/AgCl. The optimum Fc content was then applied further to investigate the pH effect, scan rate, the presence of interferences, and to determine the limit detection. To analyze the pH effect, 0.2 mM $Pb(NO_3)_2$ solution was added with 0.01M NaOH and 0.1M HCl until the pH showed pH 4 for acidic conditions and pH 8 for alkaline conditions and subjected to CV analysis at −2.5 to 2.5 V Vs Ag/AgCl. Meanwhile, various scan rates of 3, 5, and 10 mV s^{-1} were applied to see the working electrode performance on delivering current. The interference effect was studied by adding 10% Cu^{2+} and Co^{2+} solution to the $Pb(NO_3)_2$ solution. Meanwhile, limit detection was determined by applying the SPAC700-Fc to various Pb solutions of 0.05; 0.2; 0.4; and 0.8 mM. The limit of detection and quantification were determined by using equations (2) and (3), respectively. All the procedures were triple to ensure reproducibility.

$$\text{LoD} = \frac{3 \times \sigma}{m} \quad (2)$$

$$\text{LoQ} = \frac{10 \times \sigma}{m} \quad (3)$$

Where *m* is the slope of the calibration curve plot of anodic peak current versus the $Pb(NO_3)_2$ concentration, and σ is the standard deviation of the CV responses.

This research also carried out a repeatability test to determine the method's precision value. The repeatability was identified by the Repeatability Coefficient (RC), as the value of the absolute differences between two measurements, which will be at a probability of 0.95 (Nicholls, 2023). It is calculated by multiplying the subject standard deviation (S_W) or the Standard Error of Measurement (SEM) with 2.77 (Vaz *et al.*, 2013) as shown by equation (4).

$$RC = 2.77 \times S_W \quad (4)$$

3. Result and discussion

3.1 Characterization of the prepared-Carbon

The activation of coconut shell char yielded 32.6 % of the initial weight. Degradation of cellulose, hemicellulose, lignin, and unstable components in coconut shells allowed the weight loss (Wang et al., 2013). During activation, cellulose, and hemicellulose decomposition occur, increasing carbon's porosity, enhancing the oxidizing agent's diffusion into particles, and oxidizing lignin within the char (Zhou et al., 2018).

The XRD pattern of char (Fig.4) shows a broad peak centered at 2θ = 24° corresponds to the (002) and 44° corresponds to the (100) crystal plane (Bakti et al., 2018). Broad peaks confirm amorphous structures composed of randomly oriented aromatic graphene-like sheets (JCPDS#41-1487) (Siddiqui et al., 2022). Meanwhile, the XRD pattern of AC700 shows new peaks at 30°, 34°, and 35°, which are identified as chaoite or white carbon I, a carbon allotrope (Gustian et al., 2015). Those new peaks indicate the presence of graphitic phase compliance with JCPDS#22-1069 (Martínez et al., 2021; Nguyen et al., 2019). It shows that steam activation changes some amorphous to graphitic phases. Steam is able to remove disordered carbon within the solid carbon network, creating a more ordered network, new pores, and opening of clogged ones

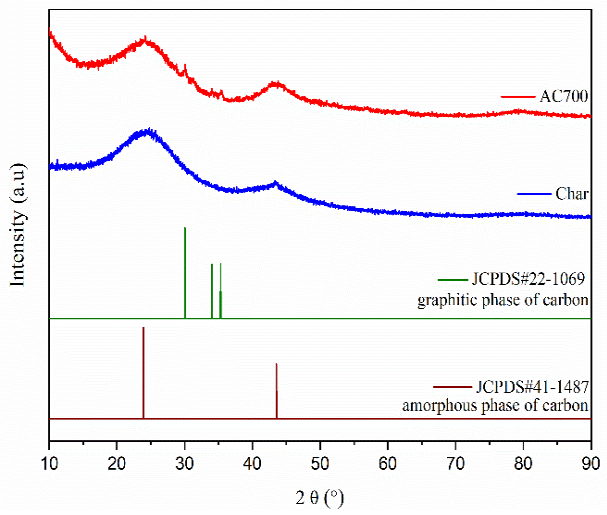

Fig 4. XRD spectra of Char and AC700

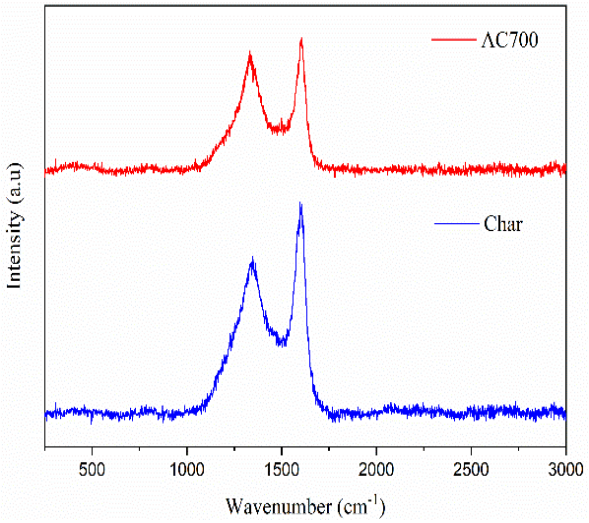

Fig 6. Raman spectra of Char and AC700

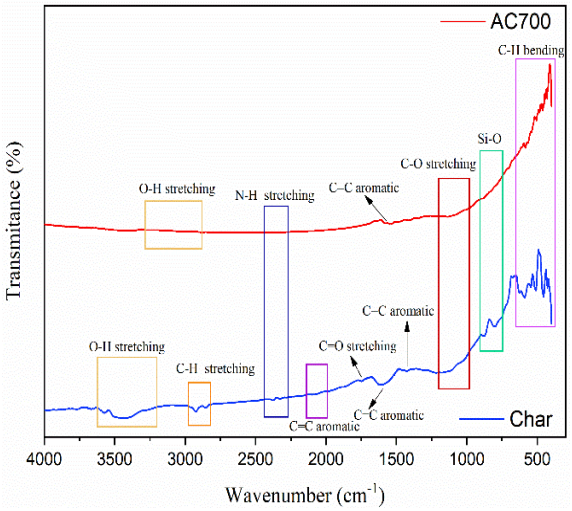

Fig 5. FTIR spectra of Char and AC700

(Mopoung & Dejang, 2021), which will increase the surface area of the carbon.

FTIR analysis found that char shows some peaks, as shown by Fig. 5, at 3292-3572 cm^{-1} belonging to O–H stretching, indicating a hydroxyl group within cellulose molecules (Rampe *et al.*, 2011). A peak at 2854-2924 cm^{-1} represents the C-H stretching, whether from hemicellulose, cellulose, and lignin (Rampe *et al.*, 2021). A peak at 2373-2285 cm^{-1} belongs to N–H bending (Das *et al.*, 2015), and at around 2076-2175 and 1440-1611 cm^{-1} belong to C=C stretching in aromatic rings (Lazim and Hadibarata, 2015). Meanwhile, a peak at 1744 cm^{-1} refers to C=O stretching, indicates ketone, carboxylic acid, and aldehydes functional groups from cellulose, hemicellulose, and lignin (Hassan *et al.*, 2021). A 1054–1115 cm^{-1} peak indicates C–O stretching of glucoside bonds from lignin (Tu *et al.*, 2021). A small peak at 806–876 cm^{-1} refers to Si–O stretching and bending, indicating the presence of silica in the coconut shell, and a small peak at 428-670 cm^{-1} belongs to C–H bending (out of plane), which indicates the presence of hydrocarbon compounds (Hakim and Sedyadi, 2020). FTIR analysis to AC700 showed that the activation caused to a lower peak intensity of O–H, C=O, C=C aromatic, C–O, C–H, and Si–O vibration, as shown by Fig. 5. It implies that the activation broke down the lignin and cellulose structure (Hakim and Sedyadi, 2020). The disappearance of the C=O peak after activation indicates the thermal decomposition of aldehyde and ketone.

Raman analysis found that the char and AC700 provide G and D-band in the range of 1597 to 1604 cm^{-1} and 1346 to 1333 cm^{-1}, respectively. Both peaks correspond to amorphous carbon (Shrestha *et al.*, 2019). Meanwhile, the D band refers to disorder and structure defects with sp^3-hybridized carbons. On the other hand, the G band corresponds to C=C stretching in graphitic carbons with sp^2 hybridized carbon systems, and the ID/IG ratio indicates the amorphous degree (Mopoung and Dejang, 2021). The ID/IG ratio of char is 0.84, a bit higher than AC700, i.e., 0.83, confirming more defects present within AC700

Fig 7. The optical image of AC700 powder **(a)**, The SEM image of AC700 **(b)**

Table 1

Specific surface area and pore volume of Char and AC700

Materials	Surface Area Multi point BET (m^2/g)	Total pores volume (L/g)	The Average of Pore Radius (nm)
Char	81.2	6.52×10^{-5}	1.60543
AC700	816.3	4.99×10^{-4}	1.22354

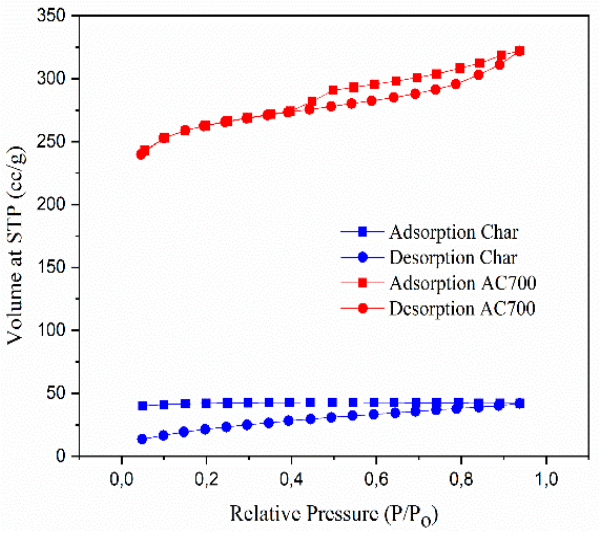

Fig 8. The isotherm profile of Char and AC700

(Lian *et al*., 2018). Breaking electroneutrality of the sp2 carbon lattice by structural defect formation effectively introducing active sites on the carbon network surface(Wu et al., 2021) improves electrocatalytic and electronic properties.

AC700 is a black powder, as shown in Fig. 7a, with a porous surface morphology (Fig 7b). The pores' shape and size are various, and the pores are mainly clean, confirming the decomposition of organic matter that blocks the pores during activation (Mopoung and Dejang, 2021).

EDX analysis shows that AC700 mainly contains 49.6% of carbon, and some minor content of oxygen, nitrogen, potassium, sulphur, sodium, and silicate at 32.42%, 10.68%, 2.48%, 1.29%, 0.79%, and 0.84%, respectively. The composition is similar to previous research on activated carbon prepared from Acacia mangium wood (Danish *et al*., 2020).

Adsorption/desorption isotherms show that AC700 follows type I (Fig. 8), indicating microporous materials with narrow pore size (< 2nm). Fig.8 also demonstrates that AC700 has an H4 type of hysteresis loop, which describes a multilayer characteristic at a relative pressure above 0.4 P/Po. The H4 hysteresis loop is usually provided by porous material consisting of narrow pore channels from microporous carbon (Zhou *et al*., 2018). BET calculation informs a total pore volume increase after activation, as listed in Table 1. It rises from 6.52×10^{-5} L/g to 4.99×10^{-4} L/g for char and AC700, respectively. Table 1 shows that char has a pore size of 1.60543 nm, which is more significant than AC700, i.e., 1.22354 nm (Table 1). However, the total pore volume of char is 80.66 % smaller than AC700 (Table 1). It indicates that activation has successfully cleaned the pores and allowed them to adsorb more N_2 gas during analysis, increasing surface area after activation. The surface area of AC700, which is activated by steam, is even higher than another method used for carbon, i.e., 516 m^2/g (Sujiono *et al*., 2022). The isotherm curve (Fig. 8) also shows that char with all organic content inside the pores seems to hardly bind the N_2 molecules, which makes it hard to be desorbed or requires more equilibrium time to result in complete desorption and provides a closed-isotherm curve.

3.2 Electrochemical performance of SPCE

Impedance measurement of AC700/Cu foil was done to understand its electrical properties. The Nyquist plot in Fig. 9(a) describes impedance data along with its R-L network model applied for data fitting. Fitting resulted in resistance, R of 11.41 Ohm, equal to 8.68×10^{-2} Scm^{-1} conductivity, indicating good charge transfer kinetics (Ambaye *et al*., 2022).

Table 2

The onset anodic potential (*E*a), the onset cathodic potential (*E*c), and the current peaks (*i*pa and *i*pc) provided by the various carbon electrod under scan rate of 10 mV s^{-1} within potential range of −1.5 to 1 V versus Ag/AgCl reference

The Electrode	*E*a (V)	*i*pa (μA)	*E*c (V)	*i*pc (μA)
SPCE Poten	− 0.27	0.00050	0.045	− 0.00075
SPAC700	− 0.27	0.00075	0.140	–0.00110
SPAC700-Fc10	− 0.24	0.00001	0.005	− 0.00025
SPAC700-Fc20	− 0.23	0.00025	0.067	− 0.00035
SPAC700-Fc30	− 0.40	0.00100	0.140	− 0.00125

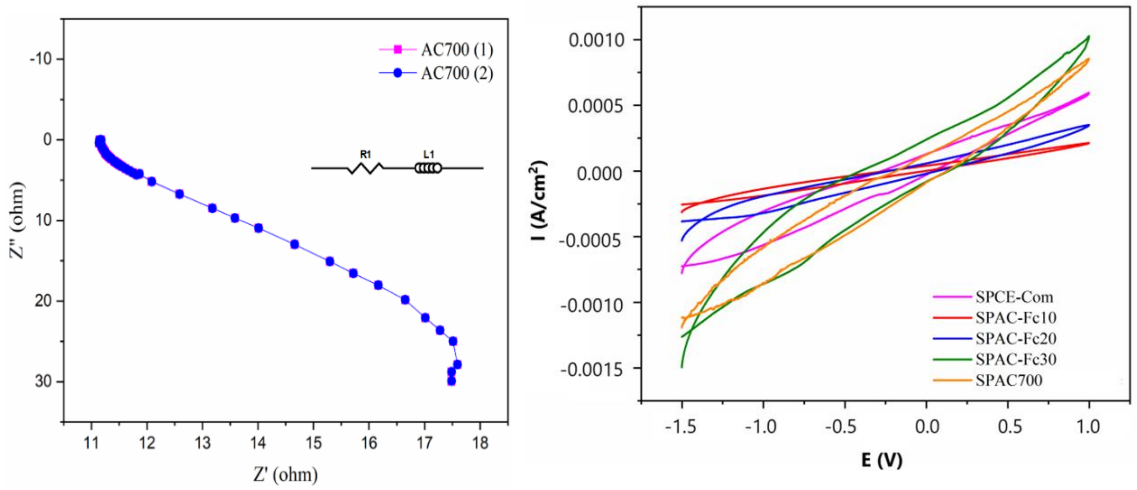

(a) (b)

Fig 9. Nyquist plots of AC700 (a), and Cyclic Voltammogram of SPAC700, SPAC700-Fc10, SPAC700-Fc20, SPAC700-Fc30, and SPCE-com in 0.03 mM $Pb(NO_3)_2$ solution within -1.5 V to 1 V vs Ag/AgCl, scan rate of 10 mVs^{-1}(b)

In the investigation of SPAC700 for electrochemical analysis, a cyclic voltammetry test was conducted on lead (II) solution. The result is compared with a commercial SPCE, SPCE-com (Table 2). Both electrodes provide a reversible curve, as described in Fig. 9(b). A 10 % and 20 % ferrocene addition also resulted in a reversible curve, but the current intensity is below the SPCE-com. The current density is even lower than SPAC700 without Fc. Molecular interaction between Fc with carbon substrate is feeble without oxidation number change. The interaction may cause the Fc molecules to intercalate into carbon network as it occurs with Fc addition to highly oriented pyrolytic graphite (Kumar et al., 2023). For amorphous carbon, intercalation may reduce the surface area, allowing lower the current conduction of the carbon. This is because the Fc units significantly change the excited-state dynamics of the substrate(Yuan et al., 2018). However, at the right amount, the Fc intercalation produces carbon defect that increases electronic conduction. This research found that 30% addition can increase current density. However, further research is needed to understand the optimum quantity of Fc to support the carbon substrate. The current density became higher when 30% Ferrocene was added to SPAC700. The oxidation starts at −0. 4 V versus Ag/AgCl, and reduces back at 0.13 vs. Ag/AgCl, indicating Pb ions reduction. Still the oxidation potential does not match with Pb oxidation, which should be around -0.071 vs Ag/AgCl (0.126 V vs SHE) (Millazo *et al.*, 1978). It is caused by a tiny amount of Pb(II) available. Meanwhile, ferrocene redox potential is approximated at around 0.527 ±0.018 V vs. Ag/Ag^+ in acetonitrile reference (Lewandowski *et al.*, 2009).

Considering high current density increases at 30% Fc, this research used SPAC700-Fc30 for further performance tests. It is recognized that ferrocene cooperates with the carbon substrate to form a more extensive conjugated system, which accelerates the electron transfer between the lead metal and the carbon electrode and increases the detection sensitivity (Beitollahi *et al.*, 2020). SEM/EDX analysis found that the Fc attached to the carbon film diffuse well without any different aggregate detected (Fig.10). However, EDX analysis found the Fe presence at 5.17 weight% among the other minor contents of oxygen, nitrogen, potassium, sulphur, sodium, and silicate. The main content is carbon with 58.49 %weight, which is higher than the C content within AC700, i.e., 49.6 %weight; because of the Fc presence, $Fe(C_5H_5)_2$ indeed increased the C content

Voltammogram response of leads oxidation revealed that anodic peak current increases as the concentration was changed from 0.05 to 0.2 mM $Pb(NO_3)_2$ solutions (Fig. 11(a)), reaching a maximum at 0.2 mM and then decreased. The results show that the maximum binding of these lead ions on the electrode surface occurs at 0.2 mM. The equivalent calibration plot, shown in Fig. 11 (b), as well as the anodic peak current expressed in the linear Eq. (5) with regression coefficient (R^2) =

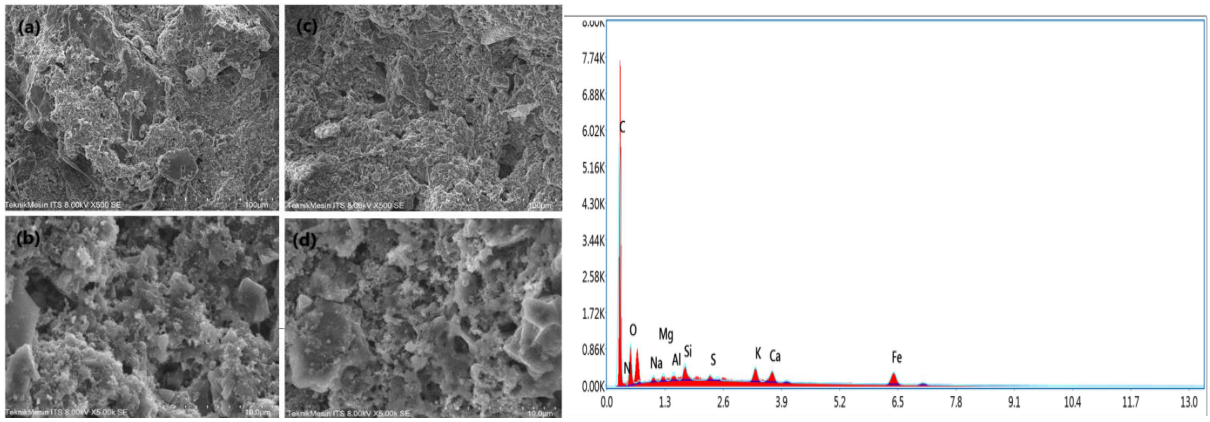

Fig. 10 SEM images of the SPAC700 (a,b) and the SPAC700-Fc30 (c,d) at different magnifications, along with the EDX result of SPAC700-Fc30

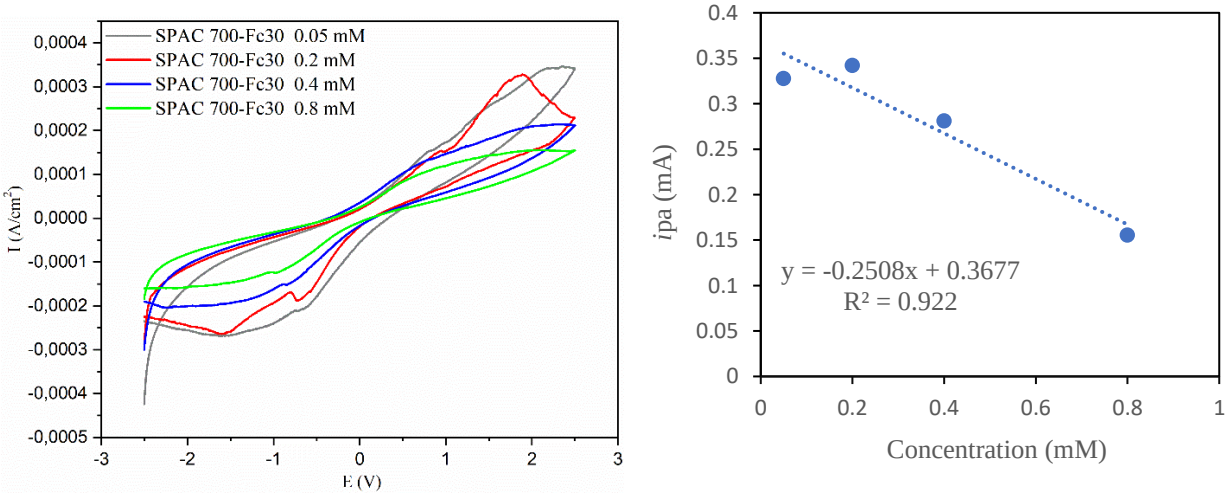

Fig 11. (a) Cyclic Voltammogram of SPAC700-Fc30 in $Pb(NO_3)_2$ solutions concentration : 0.05, 0.2, 0.4, and 0.8 mM; (b) Graph of the current response versus concentration

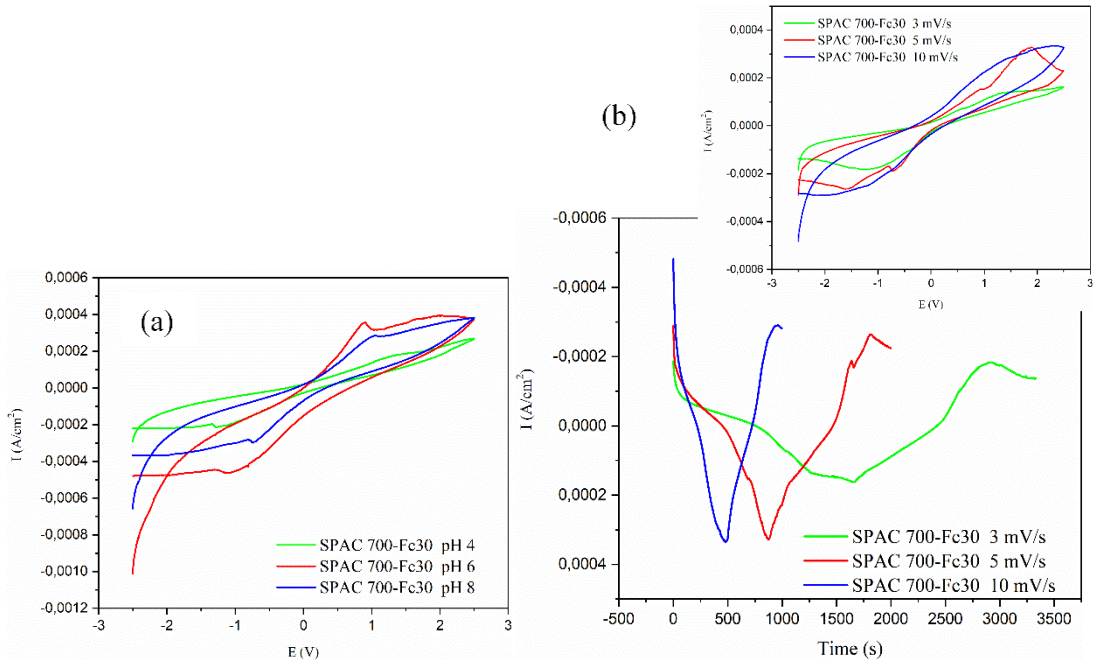

Fig 12. Cyclic Voltammogram of SPAC700-Fc30 in $Pb(NO_3)_2$ solutions at various pH of 4.0, 6.0, and 8.0 (a), and Cyclic Voltammogram (inserted) and plot of current density (I) versus scanning time of $Pb(NO_3)_2$ solutions with SPAC700-FC30 at various scan rate of 3, 5, and 10 mVs^{-1}(b)

0.922. The measurement was conducted twice with average anodic peak of (0.275±0.030) $mAcm^{-2}$ for 0.2 mM.

$$ipa\,(\mu A) = 0.2508\,(mM) + 0.3677\,(R^2 = 0.922) \quad (5)$$

Likewise, the LoD and LoQ of the SPAC700-Fc30 electrode towards detection of lead ions were calculated using Eq. (2) and (3), respectively, with a slope of linear regression (Fig 10(b)). The LoD and LoQ of SPAC700-Fc30 are 0.35 and 1.17 mM, respectively. The SPAC700-FC30 performance is compared with other published electrodes, as in Table 3. The SPAC700-Fc30 attributed a lower LOD (0.35 mM) than the others, such as tetra-tert-butyl phthalocyanine (PcH_2-tBu)/carbon (C): PcH_2-tBu/C for acetic acid detection in a buffered condition with LOD of 7.76 mM (Ndiaye *et al.*, 2016). Screen-printed electrode (SPE) with silver ink for determination of chloride ions in serum and sweat with LOD of 1 mM (Cinti *et al.*, 2018). In accordance to lead ions detection, research with a three separated electrodes system with Bismuth oxide- diphenyl thiocarbazone modified Carbon Paste Electrode (Bi-Di-CPE) found a lower LoD of 0.15 μgL^{-1} through a differential pulse voltammetry method (Yang et al., 2020). A Differential pulse voltammetry is advantageous for a deficient analyte concentration; however because of a double layer capacitance subtraction in DPV measurement, the analysis may not be sensitive to higher concentration (mM scales) in terms of Ampere per molar of the analytes (Bhavik A. Patel, 2020). Meanwhile, research on a screen-printed electrode (SPE) informs a preparation from a commercial carbon ink modified with 1,2 Dihydroxybenzene (Cathecol). In lead analysis by chronopotentiometry, the lead ions are reduced first for several time to cathode, and then stripped back at constant current. The research used three-electrode system of working (the

Table 3

Comparison of Present Work to Other Electrochemical Sensor

The Electrode	Technique and Method	Detection Method	Analyte/ Sample	Analytical Characteristic	References
tetra-tert-butyl phthalocyanine (PcH_2-tBu)/Carbon (C)	Dropcast-deposited	Cyclic Voltammetry	Volatiles Fatty Acids (VFAs)	L.R: 100-400 mM LOD: 25.77 mM	(Ndiaye *et al.*, 2016)
Patterned waxed paper screen-printed with silver ink	Electrochemical oxidation in the presence of silver	Cyclic Voltammetry	Chloride/ serum, sweat	L.R: 10-200 mM LOD: 1 mM	(Cinti *et al.*, 2018)
Fe_3O_4@AuNPs@SiO_2 MIP /Whatman paper/CPE	3D-ePAD Direct oxidation	Linear Sweep Voltammetry	Serotonin/ capsule, urine	L.R: 0.01–1,000 mM LOD: 0.002 mM	(Amatatongchai *et al.*, 2019)
ChOx/PB/CBNPs/office paper SPE	Inhibition of ChOx activity	Amperometry (H_2O_2)	Sulphur mustard (Yprite)	L.R: 1–4 mM LOD: 0.9 mM	(Colozza *et al.*, 2019)
Graphite Ink Combination with Polystyrene	Fabricated using the painting technique on PVC Paper	Cyclic Voltammetry	Uric Acid	L.R: 0.01-0.08 mM LOD: 0.0019 mM	(Wahyuni *et al.*, 2021)
Pencil graphite electrode (PGE)/ 2-amino-5-mercapto-1,3,4-thiadiazole (AMT)	Electropolymerization in an acidic medium	Differential Pulse Voltammetry	Hydrazine	L.R: 1.5-167.42 mM LOD: 25.77 mM	(Antherjanam and Saraswathyamma, 2022)
Unmodified SPCE-based sensor	Fabricated using the painting technique on polyethylene terephthalate (PET) substrate	Cyclic Voltammetry	Bisphenol A (BPA)	L.R: 0-1.0 mM LOD: 0.06 mM	(Hernández-Gordillo *et al.*, 2023)
Au-MoA-D4-GlutOX	Immobilization Enzyme	Cyclic Voltammetry	Glutamate	L.R: 5-25 mM LOD: 1.9 mM	(Urbanowicz *et al.*, 2023)
1,2 Dihydroxybenzene (Cathecol)-modified Screen- Printed Electrode.	1,2- The SPE was made from a commercial carbon ink electrodag PF-407A. Electrodeposition methode of cathecol modification	Stripping Chrono Potentiometric Three electrodes system of SPE working electrode, carbon counter electrode, and Ag/AgCl reference electrode	Lead ions	L.R: 0.1- 0.5 μg L^{-1} (0.4 – 2.4) x10^{-6} mM LOD: 0.063 μg L^{-1} (0.3 x 10^{-6} mM)	(Parat et al., 2023)
Bismuth oxide, diphenyl thiocarbazone-Carbon Paste Electrode (Bi-Di-CPE)	Carbon paste applied to a carbon rod electrode	Differential Pulse Voltammetry. 3 separated-electrodes system with Bi-Di-CPE working electrode, Standard Calomel Electrode reference, and the platinum counter electrode	Lead ions	L.R: (2.4 – 3.86) x10^{-4} mM (5-80 μgL^{-1}) LOD: 2.7 x 10^{-7} mM (0.15 μgL^{-1})	(Yang et al., 2020)
SPAC700-Fc 30%	Fabricated using the painting technique on PVC Paper	Cyclic Voltammetry A single SPCE system consisting working, counter, and reference electrodes in a piece	Lead ions	L.R: 0.05-0.8 mM LOD: 0.35 mM	**This Work**

prepared-SPE), carbon counter electrode, and Ag/AgCl reference electrode to analyze the sample(Parat et al., 2023). The stripping method provides better performance for very low concentration, but has disadvantage for a higher analyte

concentration because the analysis depends on time to deposit the analyte at the very first time before stripped back to ions. In addition, two previous researches used three-electrode system that needed more specific electrochemical chamber, a specific pre-treatment, and were less-portable. This research offers a single piece consisting of three electrodes, and this research used biomass to prepare the carbon as raw material. Other comparative works are also listed in Table 3.

Due to the analyte solution being water-base, water molecules may undergo a redox reaction, allowing pH change. Therefore, it is essential to investigate the pH effect on the analysis performance. This research applied a pH range of 4.0−8.0 by considering acid to base condition. The result is depicted in Figure 12(a), which shows an increasing current density from pH 4 to 6, and then the current decreased at pH 8. The results show that a reaction between ferrocene and lead ions occurred. The dissolution peak current is higher at pH 4 because of the existence of H^+ increased conductivity of the electrolyte. Meanwhile, when the condition turned to basic at pH 8, a slight shifting starting potential occurred due to Pb^{2+} hydrolysis (Zhang *et al.*, 2023).

This research also investigated a various scan rate of 3, 5, 10 mV s^{-1}, the results are shown in Fig. 12(b). The current response increases proportionally as the scan rate increases, indicating a good working electrode response to deliver current (Herawati *et al.*, 2017) and referring to a diffusion-controlled mechanism for reaction (Safaei et al., 2019) at the surface of SPAC700-Fc30. Scan rate of 3 mVs^{-1} was too low to produce a high current density. Meanwhile, 10 mVs^{-1} was too fast to provide a well-defined anodic and cathodic peak. A 5 mVs^{-1} scan rate seems to be the right speed to run the analysis. The potential peaks, *E*pa and *E*pc, are relatively constant, confirming a stable performance of SPAC700-Fc30 under a slightly different scan rate.

Interference test in lead ions analysis with SPAC700-Fc30 was done by adding 10% (v/v) of 0.2 mM Cu^{2+} and Co^{2+} solution into the analyte lead solution. Fig. 13 shows voltammograms, that has similar onset potential for anodic part of -0.13 V vs Ag/AgCl. However, the onset cathodic potential shift to 0.22 V from the initial 0.13 V vs Ag/AgCl by the presence of 10% Cu^{2+} solution. It indicates that the presence of 10% Co^{2+} did not disturb the measurement, however, the presence of higher Cu^{2+} concentration will matter, even though

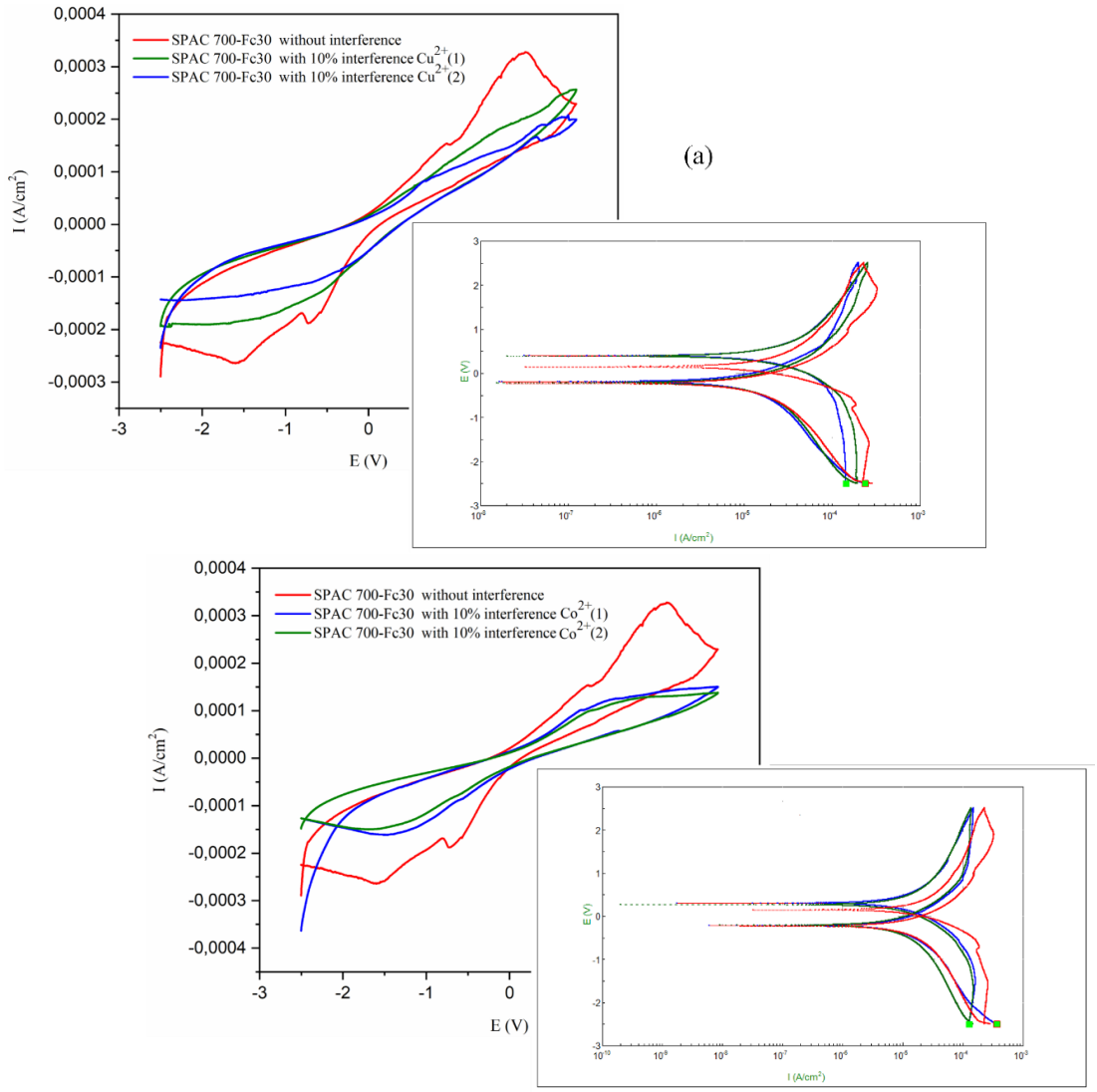

Fig 13. Cyclic voltammogram of 0.2 mM of $Pb(NO_3)_2$ solution with SPAC700-Fc30 under 10% volume of interference (green and blue curve) and without interference (red curve). The interference is 0.2 mM of $CuCl_2$ (a) and 0.2 mM of $CoCl_2.6H_2O$ (b). Plot of *E* versus log *I* is inserted confirming onset potential

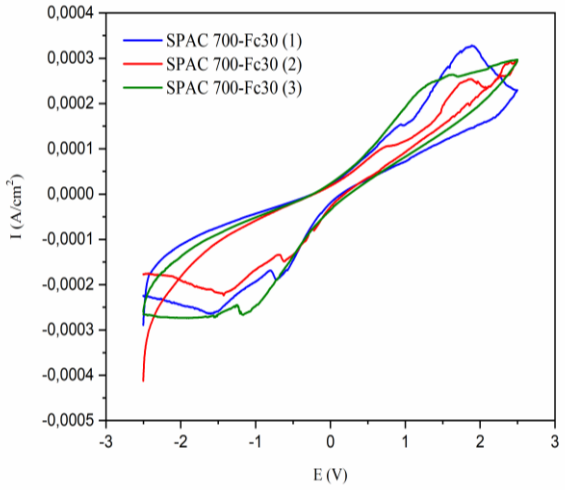

Fig 14. Cyclic Voltammogram of 0.2 mM $Pb(NO_3)_2$ solution with SPAC700-Fc30 as electrode. The analysis was conducted triple to check reproducibility at 5 m Vs^{-1} of scan rate

it still defines similar anodic pattern. The interference test was run twice to ensure similar result with the average anodic peak of (0.037±0.0022) $mAcm^{-2}$ for Cu^{2+} interference, and the average anodic peak of (0.039±0.0002) $mAcm^{-2}$ for Co^{2+} interference. Theoretically, Cu^{2+} will be reduced at 0.09 V vs Ag/AgCl, meanwhile Co^{2+} at -0.54 vs Ag/AgCl(Prakash et al., 2014), but those two peaks are not available within the CV curves (Fig.13). It is also confirmed by E(V) versus log I plot as inserted in Fig. 13, which shows a similar reduction–oxidation potential, *E*o. It indicates that SPAC700-Fc30 provides selective lead ion determination. However, further studies on the type and quantity of interference are essential since some water contaminants can change the anodic peak, as was found by previous research in hydrazine and hydroxylamine determination (Antherjanam and Saraswathyamma, 2022).

A reproducibility study is essential for a mass production plan. This research tested three pieces of SPAC700-Fc30 analyte 0.2 mM Pb solution under 5 mVs^{-1}. The result is depicted in Fig. 14. The voltammograms are identical, with *I*a of 0.25±0.008 mA cm^{-2} and *I*c of 0.34±0.09 mA cm^{-2} at the similar onset potential. The repeatability coefficient RC is 0.081, which is <<1, indicating good repeatability (Nicholls, 2023). The three times measurement also falls within 99% probability.

4. Conclusion

This research found that steam activation successfully activates the carbon produced from coconut shell char. The activation increased carbon's surface area and pore volume of the carbon, removing C=O vibration, indicating the thermal decomposition of the aldehyde and ketone group in the coconut shell. The activated carbon AC700 provides a high electrical conductivity of $8.68x10^{-2}$ S cm^{-1}, showing good electrode material potential. It is proven by the performance of the prepared SPCE from the AC700 (SPAC700) compared with the commercial SPCE. Furthermore, adding of 30% ferrocene to the working electrode, WE, part producing SPAC700-Fc30, even increases the electrochemical performance as the analytical electrode for lead ions detection, proven by the significant increase of current density (*I*pa and *I*pc). The SPAC700-Fc30 exhibited a linear range of 0.05 mM–0.8 mM with LoD of 0.35 mM and a LoQ 1.17 mM. Additionally, the SPAC700-Fc30 demonstrated excellent repeatability and consistent results under the presence of 10% interference and provides good stability towards the electrochemical sensing of lead ions.

Acknowledgement

Authors thank Sebelas Maret University for funding this research under the scheme of PUT-UNS contract number 228/UN27.22/PT.01.03/2023.

References

Ahammad, A. J. S., Pal, P. R., Shah, S. S., Islam, T., Mahedi Hasan, M., Qasem, M. A. A., Odhikari, N., Sarker, S., Kim, D. M., & Abdul Aziz, M. (2019). Activated jute carbon paste screen-printed FTO electrodes for nonenzymatic amperometric determination of nitrite. *Journal of Electroanalytical Chemistry*, *832*(November 2018), 368–379. https://doi.org/10.1016/j.jelechem.2018.11.034

Amatatongchai, M., Sitanurak, J., Sroysee, W., Sodanat, S., Chairam, S., Jarujamrus, P., Nacapricha, D., & Lieberzeit, P. A. (2019). Highly sensitive and selective electrochemical paper-based device using a graphite screen-printed electrode modified with molecularly imprinted polymers coated Fe3O4@Au@SiO2 for serotonin determination. *Analytica Chimica Acta*, *1077*, 255–265. https://doi.org/10.1016/j.aca.2019.05.047

Ambaye, A. D., Kefeni, K. K., Kebede, T. G., Ntsendwana, B., Mishra, S. B., & Nxumalo, E. N. (2022). Cu-MOF/N-doped GO nanocomposites modified screen-printed carbon electrode towards detection of 4-nitrophenol. *Journal of Electroanalytical Chemistry*, *919*(February), 116542. https://doi.org/10.1016/j.jelechem.2022.116542

Antherjanam, S., & Saraswathyamma, B. (2022). Simultaneous electrochemical determination of hydrazine and hydroxylamine on a thiadiazole derivative modified pencil graphite electrode. *Materials Chemistry and Physics*, *275*(July 2021), 125223. https://doi.org/10.1016/j.matchemphys.2021.125223

Bakti, A. I., Gareso, P. L., & Rauf, N. (2018). Characterization of Active Carbon from Coconut Shell using X-Ray Diffraction (X-RD) and SEM-EDX Techniques. *Jurnal Penelitian Fisika Dan Aplikasinya (JPFA)*, *8*(2), 115. https://doi.org/10.26740/jpfa.v8n2.p115-122

Beitollahi, H., Khalilzadeh, M. A., Tajik, S., Safaei, M., Zhang, K., Jang, H. W., & Shokouhimehr, M. (2020). Recent Advances in Applications of Voltammetric Sensors Modified with Ferrocene and Its Derivatives. *ACS Omega*, *5*(5), 2049–2059. https://doi.org/10.1021/acsomega.9b03788

Bhavik A. Patel. (2020). *Electrochemistry for Bioanalysis* (K. Eryilmaz (ed.)). Elsevier Inc.

Chairunnisa, Miksik, F., Miyazaki, T., Thu, K., Miyawaki, J., Nakabayashi, K., Wijayanta, A. T., & Rahmawati, F. (2021). Development of biomass based-activated carbon for adsorption dehumidification. *Energy Reports*, *7*, 5871–5884. https://doi.org/10.1016/j.egyr.2021.09.003

Chen, B., Xie, Q., Zhang, S., Lin, L., Zhang, Y., Zhang, L., Jiang, Y., & Zhao, M. (2021). A novel electrochemical molecularly imprinted senor based on CuCo2O4@ biomass derived carbon for sensitive detection of tryptophan. *Journal of Electroanalytical Chemistry*, *901*(May), 115680. https://doi.org/10.1016/j.jelechem.2021.115680

Cinti, S., Fiore, L., Massoud, R., Cortese, C., Moscone, D., Palleschi, G., & Arduini, F. (2018). Low-cost and reagent-free paper-based device to detect chloride ions in serum and sweat. *Talanta*, *179*(July 2017), 186–192. https://doi.org/10.1016/j.talanta.2017.10.030

Colozza, N., Kehe, K., Dionisi, G., Popp, T., Tsoutsoulopoulos, A., Steinritz, D., Moscone, D., & Arduini, F. (2019). A wearable origami-like paper-based electrochemical biosensor for sulfur mustard detection. *Biosensors and Bioelectronics*, *129*(December 2018), 15–23. https://doi.org/10.1016/j.bios.2019.01.002

Danish, M., Akhtar, M. N., Hashim, R., Saleh, J. M., & Bakar, E. A. (2020). Analysis using image segmentation for the elemental

composition of activated carbon. *MethodsX*, *7*, 1–9. https://doi.org/10.1016/j.mex.2020.100983

Das, D., Samal, D. P., & BC, M. (2015). Preparation of Activated Carbon from Green Coconut Shell and its Characterization. *Journal of Chemical Engineering & Process Technology*, *06*(05). https://doi.org/10.4172/2157-7048.1000248

El Hamdouni, Y., El Hajjaji, S., Szabó, T., Trif, L., Felhősi, I., Abbi, K., Labjar, N., Harmouche, L., & Shaban, A. (2022). Biomass valorization of walnut shell into biochar as a resource for electrochemical simultaneous detection of heavy metal ions in water and soil samples: Preparation, characterization, and applications. *Arabian Journal of Chemistry*, *15*(11). https://doi.org/10.1016/j.arabjc.2022.104252

Emambakhsh, F., Asadollahzadeh, H., Rastakhiz, N., & Mohammadi, S. Z. (2022). Highly sensitive determination of Bisphenol A in water and milk samples by using magnetic activated carbon – Cobalt nanocomposite-screen printed electrode. *Microchemical Journal*, *179*(August 2021), 107466. https://doi.org/10.1016/j.microc.2022.107466

Gustian, I., Angasa, E., Agustini, D., Maryanti, E., & Fitriani, D. (2015). Preparation of Fe-intercalated Graphite Based on Coal Tailings, Dimensional Structure. *Aceh International Journal of Science and Technology*, *4*(3), 88–92. https://doi.org/10.13170/aijst.4.3.3017

Hakim, L., & Sedyadi, E. (2020). Synthesis and Characterization of Fe3O4 Composites Embeded on Coconut Shell Activated Carbon. *JKPK (Jurnal Kimia Dan Pendidikan Kimia)*, *5*(3), 245. https://doi.org/10.20961/jkpk.v5i3.46543

Hassan, U. F., Sallau, A. A., Ekanem, E. O., Jauro, A., & Kolo, A. M. (2021). Effect of carbonization temperature on properties of char from coconut shell. *Industrial Crops and Products 9*(1), 34–39. https://doi.org/10.1016/j.indcrop.2008.02.012

Herawati, Buchari, B., & Noviandri, I. (2017). Characterization of Reference Electrode Ag / Agcl. *Conference Paper : 3rd International Seminar on Education Technology 2017*, *3*(1 mm), 22–26.

Hernández-Gordillo, M. J., Alvarez-Serna, B. E., & Ramírez-Chavarría, R. G. (2023). Unmodified Screen-Printed Electrodes-Based Sensor for Electrochemical Detection of Bisphenol A. *IFMBE Proceedings*, *86*(October), 603–610. https://doi.org/10.1007/978-3-031-18256-3_63

Hidayat, A., & Sutrisno, B. (2016). Comparison on pore development of activated carbon produced by chemical and physical activation from palm empty fruit bunch. *IOP Conference Series: Materials Science and Engineering*, *162*(1). https://doi.org/10.1088/1757-899X/162/1/012008

Huang, L., Wang, S., Zhang, Y., Huang, X. H., Peng, J. J., & Yang, F. (2021). Preparation of a N-P co-doped waste cotton fabric-based activated carbon for supercapacitor electrodes. *Xinxing Tan Cailiao/New Carbon Materials*, *36*(6), 1128–1137. https://doi.org/10.1016/S1872-5805(21)60054-9

Imani, S., Alizadeh, A., Roudgar-Amoli, M., & Shariatinia, Z. (2022). Bi-layered photoelectrodes of TiO2/activated carbon modified with SrTiO3 films boosted sunlight harvesting of dye-sensitized solar cells. *Inorganic Chemistry Communications*, *145*(August), 110045. https://doi.org/10.1016/j.inoche.2022.110045

Jagirani, M. S., Balouch, A., Mahesar, S. A., Alveroğlu, E., Kumar, A., Tunio, A., & Abdullah. (2022). Selective and sensitive detoxification of toxic lead ions from drinking water using lead (II) ion-imprinted interpenetrating polymer linkage. *Polymer Bulletin*, *79*(3), 1887–1909. https://doi.org/10.1007/s00289-021-03546-8

Khuong, D. A., Nguyen, H. N., & Tsubota, T. (2021). Activated carbon produced from bamboo and solid residue by CO2 activation utilized as CO2 adsorbents. *Biomass and Bioenergy*, *148*(February), 106039. https://doi.org/10.1016/j.biombioe.2021.106039

Kuan-Ching Lee, Mitchell Shyan Wei Lim, Zhong-Yun Hong, S. C. G.-T. P. and C.-M. H. (2021). Coconut Shell-Derived Activated Carbon for High-Performance. *Energies*, *14*(15), 4546.

Kumar, A., Kumar, A., & Anwesha. (2023). Effect of substrate on interfacial electronic properties of ferrocene thin films. *Materials Today: Proceedings*, *80*, 544–548. https://doi.org/10.1016/j.matpr.2022.11.044

Lazim, Z. M., & Hadibarata, T. (2015). *Adsorption Characteristics of Bisphenol A onto Low-Cost Modified Phyto- Waste Material in Aqueous Solution Adsorption Characteristics of Bisphenol A onto Low-Cost Modified Phyto-Waste Material in Aqueous Solution*. *May 2020*. https://doi.org/10.1007/s11270-015-2318-5

Lewandowski, A., Waligora, L., & Galinski, M. (2009). Ferrocene as a reference redox couple for aprotic ionic liquids. *Electroanalysis*, *21*(20), 2221–2227. https://doi.org/10.1002/elan.200904669

Lian, X., Li, Q., Zhao, Y., Liu, S., Liu, H., & Zhang, H. (2018). The electrochemical properties of porous carbon derived from the prawn as anode for lithium ion batteries. *International Journal of Electrochemical Science*, *13*(3), 2474–2482. https://doi.org/10.20964/2018.03.33

Liu, Y., Chang, C., Xue, Q., Wang, R., Chen, L., Liu, Z., & He, L. (2022). Highly efficient detection of Pb(II) ion in water by polypyrrole and metal-organic frame modify glassy carbon electrode. *Diamond and Related Materials*, *130*(October), 109477. https://doi.org/10.1016/j.diamond.2022.109477

Liu, Z., Wang, R., Xue, Q., Chang, C., Liu, Y., & He, L. (2023). Highly efficient detection of Cd(II) ions in water by graphitic carbon nitride and tin dioxide nanoparticles modified glassy carbon electrode. *Inorganic Chemistry Communications*, *148*(November 2022), 110321. https://doi.org/10.1016/j.inoche.2022.110321

Mao, D., Duan, P., & Piao, Y. (2022). Acid phosphate-activated glassy carbon electrode for simultaneous detection of cadmium and lead. *Journal of Electroanalytical Chemistry*, *925*(October), 116898. https://doi.org/10.1016/j.jelechem.2022.116898

Martínez, R. R. G., González, C. A. R., Hernández-Paz, J. F., Vega, F. J., Montes, H. C., & Armendáriz, I. O. (2021). Synthesis and characterization of carbon aerogels electrodes modified by ag2s nanoparticles. *Materials Research*, *24*(3), 3–8. https://doi.org/10.1590/1980-5373-MR-2020-0387

Millazo, G., Caroli, S., & Sharma, V. K. (1978). Standard Reduction Potentials by Element. In *Tables of Standard Electrode Potentials* (pp. 1–15). Wiley, London.

Mopoung, S., & Dejang, N. (2021). Activated carbon preparation from eucalyptus wood chips using continuous carbonization-steam activation process in a batch intermittent rotary kiln. *Scientific Reports* |, *11*(1), 13948. https://doi.org/10.1038/s41598-021-93249-x

Mopoung, S., Sitthikhankaew, R., & Mingmoon, N. (2021). Preparation of anode material for lithium battery from activated carbon. *International Journal of Renewable Energy Development*, *10*(1), 91–96. https://doi.org/10.14710/ijred.2021.32997

Ndiaye, A. L., Delile, S., Brunet, J., Varenne, C., & Pauly, A. (2016). Electrochemical sensors based on screen-printed electrodes: The use of phthalocyanine derivatives for application in VFA Detection. *Biosensors*, *6*(3). https://doi.org/10.3390/bios6030046

Nguyen, H., Sung, Y., O'Shaughnessy, K., Shan, X., & Shih, W.-C. (2018). Smartphone Nanocolorimetry for On-Demand Lead Detection and Quantitation in Drinking Water. *Analytical Chemistry*, *90*(19), 11517–11522. https://doi.org/10.1021/acs.analchem.8b02808

Nguyen, L. H., Nguyen, T. M. P., Van, H. T., Vu, X. H., Ha, T. L. A., Nguyen, T. H. V., Nguyen, X. H., & Nguyen, X. C. (2019). Treatment of Hexavalent Chromium Contaminated Wastewater Using Activated Carbon Derived from Coconut Shell Loaded by Silver Nanoparticles: Batch Experiment. *Water, Air, and Soil Pollution*, *230*(3). https://doi.org/10.1007/s11270-019-4119-8

Nicholls, R. (2023). *Statistics in R: Repeatability Coefficient*. [WWW Document].

Nita, C., Zhang, B., Dentzer, J., & Matei Ghimbeu, C. (2021). Hard carbon derived from coconut shells, walnut shells, and corn silk biomass waste exhibiting high capacity for Na-ion batteries. *Journal of Energy Chemistry*, *58*, 207–218. https://doi.org/10.1016/j.jechem.2020.08.065

Parat, C., Ricard, E., Mefteh, W. Ben, & Hécho, I. Le. (2023). Carbon screen-printed electrodes modified by a polycatechol film for Cu and Pb detection in acidified drinking water. *Electrochimica Acta*, *461*(December 2022). https://doi.org/10.1016/j.electacta.2023.142666

Prakash, V., Sun, Z., Sietsma, J., & Yang, Y. (2014). Electrochemical Recovery of Rare Earth Elements from Magnet Scraps- A Theoretical Analysis. *ERES2014: 1st European Rare Earth*

Resources Conference|Milos|04-07/09/2014, 163–170. https://www.researchgate.net/publication/322937071_Electrochemical_recovery_of_Rare_Earth_Elements_from_Magnet_scrap-_A_theoretical_analysis/link/5a78797aaca2722e4df30330/download

Rahmawati, F., Heliani, K. R., Wijayanta, A. T., Zainul, R., Wijaya, K., Miyazaki, T., & Miyawaki, J. (2023). Alkaline leaching-carbon from sugarcane solid waste for screen-printed carbon electrode. *Chemical Papers*. https://doi.org/10.1007/s11696-023-02712-8

Rahmawati, F., Ridassepri, A. F., Chairunnisa, Wijayanta, A. T., Nakabayashi, K., Miyawaki, J., & Miyazaki, T. (2021). Carbon from bagasse activated with water vapor and its adsorption performance for methylene blue. *Applied Sciences (Switzerland)*, *11*(2), 1–16. https://doi.org/10.3390/app11020678

Rampe, M. J., Santoso, I. R. S., Rampe, H. L., Tiwow, V. A., & Apita, A. (2021). Infrared Spectra Patterns of Coconut Shell Charcoal as Result of Pyrolysis and Acid Activation Origin of Sulawesi, Indonesia. E3S Web Conf. 328, 08008, https://doi.org/10.1051/e3sconf/202132808008.

Rampe, M. J., Setiaji, B., Trisunaryanti, W., & Triyono, T. (2011). Fabrication and Characterization of Carbon Composite From Coconut Shell Carbon. *Indonesian Journal of Chemistry*, *11*(2), 124–130. https://doi.org/10.22146/ijc.21398

Ren, S., Zeng, J., Zheng, Z., & Shi, H. (2021). Perspective and application of modified electrode material technology in electrochemical voltammetric sensors for analysis and detection of illicit drugs. *Sensors and Actuators, A: Physical*, *329*, 112821. https://doi.org/10.1016/j.sna.2021.112821

Rezma, S., Birot, M., Hafiane, A., & Deleuze, H. (2017). Physically activated microporous carbon from a new biomass source: Date palm petioles. *Comptes Rendus Chimie*, *20*(9–10), 881–887. https://doi.org/10.1016/j.crci.2017.05.003

Ridassepri, A. F., Rahmawati, F., Heliani, K. R., Miyawaki, J., & Wijayanta, A. T. (2020). Activated Carbon from Bagasse and its Application for Water Vapor Adsorption. *Evergreen Joint Journal of Novel Carbon Resource & Green Asia Strategy*, *07*(03), 409–416. https://doi.org/10.5109/4068621

Rizal, W. A., Nisa, K., Maryana, R., Prasetyo, D. J., Pratiwi, D., Jatmiko, T. H., Ariani, D., & Suwanto, A. (2020). Chemical composition of liquid smoke from coconut shell waste produced by SME in Rongkop Gunungkidul. *IOP Conference Series: Earth and Environmental Science*, *462*(1). https://doi.org/10.1088/1755-1315/462/1/012057

Safaei, M., Beitollahi, H., & Shishehbore, M. R. (2019). Modified screen printed electrode for selective determination of folic acid. *Acta Chimica Slovenica*, *66*(4), 777–783. https://doi.org/10.17344/acsi.2018.4629

Shrestha, L., Thapa, M., Shrestha, R., Maji, S., Pradhananga, R., & Ariga, K. (2019). Rice Husk-Derived High Surface Area Nanoporous Carbon Materials with Excellent Iodine and Methylene Blue Adsorption Properties. *C*, *5*(1), 10. https://doi.org/10.3390/c5010010

Siddiqui, M. F., Khan, S. A., Hussain, D., Tabrez, U., Ahamad, I., Fatma, T., & Khan, T. A. (2022). A sugarcane bagasse carbon-based composite material to decolor and reduce bacterial loads in waste water from textile industry. *Industrial Crops and Products*, *176*(November 2021), 114301. https://doi.org/10.1016/j.indcrop.2021.114301

Su, S. fen, Ye, L. meng, Tian, Q. mei, Situ, W. bei, Song, X. liang, & Ye, S. ying. (2020). Photoelectrocatalytic inactivation of Penicillium expansum spores on a Pt decorated TiO2/activated carbon fiber photoelectrode in an all-solid-state photoelectrochemical cell. *Applied Surface Science*, *515*(February), 145964. https://doi.org/10.1016/j.apsusc.2020.145964

Sujiono, E. H., Zabrian, D., Zurnansyah, Mulyati, Zharvan, V., Samnur, & Humairah, N. A. (2022). Fabrication and characterization of coconut shell activated carbon using variation chemical activation for wastewater treatment application. *Results in Chemistry*, *4*, 100291. https://doi.org/10.1016/j.rechem.2022.100291

Tu, W., Liu, Y., Xie, Z., Chen, M., Ma, L., Du, G., & Zhu, M. (2021). A novel activation-hydrochar via hydrothermal carbonization and KOH activation of sewage sludge and coconut shell for biomass wastes: Preparation, characterization and adsorption properties. *Journal of Colloid and Interface Science*, *593*, 390–407. https://doi.org/10.1016/j.jcis.2021.02.133

Urbanowicz, M., Sadowska, K., Lemieszek, B., Paziewska-Nowak, A., Sołdatowska, A., Dawgul, M., & Pijanowska, D. G. (2023). Effect of dendrimer-based interlayers for enzyme immobilization on a model electrochemical sensing system for glutamate. *Bioelectrochemistry*, *152*(March). https://doi.org/10.1016/j.bioelechem.2023.108407

Vaz, S., Falkmer, T., Passmore, A. E., Parsons, R., & Andreou, P. (2013). The Case for Using the Repeatability Coefficient When Calculating Test-Retest Reliability. *PLoS ONE*, *8*(9), 1–7. https://doi.org/10.1371/journal.pone.0073990

Wahyuni, W. T., Putra, B. R., Heryanto, R., Rohaeti, E., Yanto, D. H. Y., & Fauzi, A. (2021). A Simple Approach to Fabricate a Screen-Printed Electrode and Its Application for Uric Acid Detection. *International Journal of Electrochemical Science*, *16*(2), 1–14. https://doi.org/10.20964/2021.02.36

Wang, Q., Zhao, H. H., Chen, J. W., Gu, K. D., Zhang, Y. Z., Zhu, Y. X., Zhou, Y. K., & Ye, L. X. (2009). Adverse health effects of lead exposure on children and exploration to internal lead indicator. *Science of The Total Environment*, *407*(23), 5986–5992. https://doi.org/10.1016/j.scitotenv.2009.08.038

Wang, X., Li, D., Yang, B., & Li, W. (2013). Textural characteristics of coconut shell-based activated carbons with steam activation. *Advanced Materials Research*, *608–609*, 366–373. https://doi.org/10.4028/www.scientific.net/AMR.608-609.366

Widanarto, W., Budianti, S. I., Ghoshal, S. K., Kurniawan, C., Handoko, E., & Alaydrus, M. (2022). Improved microwave absorption traits of coconut shells-derived activated carbon. *Diamond and Related Materials*, *126*(November 2021), 109059. https://doi.org/10.1016/j.diamond.2022.109059

Widyaningrum, B. A., Widianti, N., Harsini, M., & Purwaningsih, A. (2020). Selective voltammetric detection of dopamine using ferrocene modified carbon paste electrode. *IOP Conference Series: Earth and Environmental Science*, *572*(1). https://doi.org/10.1088/1755-1315/572/1/012037

Wu, Q., Yan, X., Jia, Y., & Yao, X. (2021). Defective carbon-based materials: controllable synthesis and electrochemical applications. *EnergyChem*, *3*(5), 100059. https://doi.org/10.1016/j.enchem.2021.100059

Yang, Q., Yang, C., Yi, J., Fan, G., Yang, H., & Ge, Z. (2020). A Sensitive Carbon Paste Electrode for Selective Detection of Lead Based on the Synergistic Effect of Bismuth and Chelating Agent. *ECS Journal of Solid State Science and Technology*, *9*(10), 101012. https://doi.org/10.1149/2162-8777/abb8ba

Yuan, K., Yousefalizadeh, G., Saraci, F., Peng, T., Kozin, I., Stamplecoskie, K. G., & Wang, S. (2018). Impact of Ferrocene Substitution on the Electronic Properties of BODIPY Derivatives and Analogues. *Inorganic Chemistry*, *57*(23), 14698–14704. https://doi.org/10.1021/acs.inorgchem.8b02476

Zhang, H., Li, Y., Zhang, Y., Wu, J., Li, S., & Li, L. (2023). A Disposable Electrochemical Sensor for Lead Ion Detection Based on In Situ Polymerization of Conductive Polypyrrole Coating. *Journal of Electronic Materials*, *52*(3), 1819–1828. https://doi.org/10.1007/s11664-022-10175-y

Zhou, J., Luo, A., & Zhao, Y. (2018). Preparation and characterisation of activated carbon from waste tea by physical activation using steam. *Journal of the Air and Waste Management Association*, *68*(12), 1269–1277. https://doi.org/10.1080/10962247.2018.1460282